Fibers and Polymers (2024) 25:485–500
https://doi.org/10.1007/s12221-023-00454-8

Online ISSN 1875-0052
Print ISSN 1229-9197

REGULAR ARTICLE

In Vitro Properties of Electrospun Composite Fibers Containing Boric Acid and Enhanced with Epidermal Growth Factor for Wound Dressing Applications

Habip Orhan[1] · **Bengi Yilmaz**[1,2]

Received: 16 October 2023 / Revised: 28 November 2023 / Accepted: 4 December 2023 / Published online: 11 January 2024

Abstract

The requirements of the wound microenvironment, involving pH regulation, mechanical compatibility with skin, and prevention of bacterial attachment, highlight crucial considerations for advanced wound dressings. This study focused on electrospinning of poly(L-lactide-co-ε-caprolactone) (PLCL) enriched with 3–5% boric acid particles. The fibers were also supplemented with epidermal growth factor (EGF) prior to in vitro cell culture experiments. The results revealed that the fibers, with micro-to-nano thickness, displayed unique morphologies as boric acid particles interacted with the PLCL. Boric acid-containing fibers showed lower swelling rates compared to pure PLCL fibers that achieved a swelling rate of 151 ± 10.3%. Nevertheless, they maintained slightly acidic conditions and adequate oxygen conductivity in vitro. The water vapor transmission rate (WVTR) of fibers produced using a 5% boric acid-added PLCL was measured at 557 ± 20.9 g/m^{2}day at 24 h, demonstrating competitive performance with commercial products. The incorporation of 5% boric acid in PLCL fibers significantly improved their maximum tensile stress, reaching 11.31 ± 0.82 MPa, as opposed to pure PLCL, which attained 6.92 ± 2.08 MPa. The Young's modulus values were determined as 190.53 ± 64.80 MPa for pure PLCL and 224.74 ± 91.66 MPa for PLCL containing 5% boric acid. In vitro fibroblast cell (3T3) proliferation on all fiber types did not show a significant difference compared to control. Fluorescent microscopy displayed a good adhesion and spread of cells on boric acid containing fibers. The addition of boric acid drastically reduced the attachment of *Escherichia coli*. The findings demonstrated the promising potential of electrospun PLCL fibers with incorporated boric acid as wound dressings.

Keywords Boric acid · Electrospinning · PLCL · Wound dressing · Anti-bacterial

1 Introduction

A wound dressing serves as a sterile, protective barrier that promotes the healing process by shielding injured tissues from outside, maintaining a moist environment, prevent wound surface necrosis, and facilitating oxygen permeability without dehydrating the wound [1]. It should possess mechanical properties that match those of the skin tissue to minimize the risk of mechanical trauma. The material selection for wound dressings should prioritize non-toxicity, biodegradability, and biocompatibility. Currently, various types of dressings are utilized in wound care, including fibers, sponges, hydrogels, foams, and hydrocolloids [2]. Despite the progress made in wound dressing development, it is important to note that extensive research is still needed in this field. This is because there is no universally effective and ideal dressing that can be applied in all circumstances because of the unique properties of various wound types and the different stages of wound healing [3]. For example, hydrogels with their softness, non-adherence, swellability, and support for autolytic debridement properties, are appropriate for making dressings to treat acute/chronic wounds, burns, and diabetic foot ulcers [4]. However, in some cases, the risk of maceration arises when hydrogels are used [5], since their exceptional fluid-retention capacity can cause excessive moisture to accumulate in the wound and surrounding skin, thereby weakening the skin and heightening the susceptibility to damage and infection.

✉ Bengi Yilmaz
bengi.yilmaz@sbu.edu.tr

[1] Department of Tissue Engineering, University of Health Sciences Turkey, Istanbul, Turkey

[2] Department of Biomaterials, University of Health Sciences Turkey, Istanbul, Turkey

Electrospun micro- and nanofibers are commonly employed as scaffold materials in tissue engineering mainly because they can mimic the porous structure of the natural extracellular matrix (ECM) [6]. These fibers are also well suited for topical delivery of various molecules, including drugs, antimicrobial agents, and growth factors, owing to their high surface-to-volume ratio, promoting extended retention of these substances at the wound site. Additionally, their porous, thin, and flexible structure facilitates effective gas and moisture exchange [7]. Electrospun natural polymer fibers have been attracting interest due to their high biocompatibility and biodegradability. However, these dressings are susceptible to deformation, primarily because of their high hydrophilicity and insufficient mechanical properties [8]. Additionally, their processing performance is suboptimal, and their cost is relatively high, which makes mass production challenging. On the other hand, synthetic polymers possess the advantages of better mechanical properties and cost-effectiveness. In addition, enhancing new synthetic composites might lead to the development of important properties that are comparable to those of skin, as well as the prevention of microbial penetration and the regulation of the amount of moisture in the wound environment [9].

Polycaprolactone (PCL), one of the most widely utilized synthetic polymeric biomaterial, offers low melting point, high tensile strength, non-toxicity, and biodegradability; nevertheless, it still presents certain structural challenges [10]. For instance, tissues like skin, which experience deformation, or dynamic environments like cardiac or lung tissue, require polymers with high elasticity and resilience [11]. Polylactic acid (PLA) is the most extensively investigated and employed biodegradable aliphatic polyester [12]. However, PLA, like PCL, faces challenges in providing the required elasticity and resilience for tissues that undergo deformation or are in dynamic environments. The copolyester of ε-caprolactone and lactide, poly(l-lactide-co-ε-caprolactone) (PLCL), is a synthetic, biodegradable copolymer that has received FDA approval for use in orthopedic and wound closure applications [13]. It has unusual flexibility in contrast to other biodegradable polymers, which have a tendency to be hard and brittle [14]. PLCL exhibits a rubbery elasticity due to its physically cross-linked structure, and its mechanical properties can be finely tuned by adjusting the monomer ratio [15].

Wound healing is a complex regeneration process characterized by the spatial and temporal synchronization of the inflammatory phase with tissue regeneration and remodeling [16]. The intricate process is both executed and controlled by a complex signaling network, which comprises many growth factors, cytokines, and chemokines. Within this network, the epidermal growth factor (EGF) family holds particular significance [17]. EGF is a protein that triggers cell growth and differentiation secreted by platelets, macrophages, and fibroblasts, acting locally on epithelial cells. The EGF family plays a role in epithelial wound healing by promoting keratinocyte, endothelial cell, and fibroblast stimulation, proliferation, and migration, ultimately facilitating dermal regeneration and accelerating wound healing by enhancing collagen deposition and neovascularization [18]. External EGF supplementation may promote quicker re-epithelialization, lower the risk of infection, and enhance the efficiency and effectiveness of wound healing [19].

Wound healing is also strongly related to the microenvironment of the wound. The pH value around the wound directly and indirectly influences all the biochemical reactions occurring during this healing process [20]. The natural acidic environment of the skin is disrupted in wounds where the underlying tissue is exposed, due to the different pH (pH = 7.4) of the body's internal environment [21]. Restoring the natural acidic environment on the skin can effectively assist in reducing the microbial load on the body's surface, even if they are highly resistant to antibiotics. Additionally, when pH is elevated to an alkaline state, wound healing progression decreases [22]. Therefore, the topical application of acids such as boric acid, citric acid, acetic acid, ascorbic acid, and alginic acid has been reported in various studies on wounds to control infection and promote healing [23].

While electrospun antibacterial fibers have been created using PCL and PLA with various well-known antibacterial agents, such as antibiotics, triclosan, chlorhexidine, silver nanoparticles, metal oxide nanoparticles [24] and even natural compounds like spirulina [25], there are very limited studies in the literature specifically exploring wound dressings engineered to deliver therapeutic doses of boric acid, despite its long-standing historical use in wound care as a potent antiseptic [26]. A single study investigated the use of polyurethane sponges impregnated with micron-sized boric acid particles at a concentration of 2–3%, comparing their efficacy with conventional silver nitrate-impregnated sponges for chronic wound treatment [27]. The findings revealed a substantial increase in fibroblast count, collagen synthesis, and angiogenesis among patients treated with the boric acid particle-infused sponges in conjunction with the negative pressure wound treatment system. Boric acid is also recognized as an effective antibacterial and antibiofilm agent against common bacteria, *S. aureus* and *E. coli*, both of which are significant factors in wound infections [28]. It has demonstrated significant antifungal activity against various clinically relevant *Candida* species and has proven effective, particularly at a concentration of 5% [29]. In line with these findings, a fibrous wound dressing comprising polyamide 6/honey/boric acid was previously fabricated through an electrohydrodynamic process [30]. This approach leveraged the synergistic effect of boric acid solution and pine honey, demonstrating antibacterial efficacy against both *S. aureus* and *E. coli*. Furthermore, the significance of boric acid in

wound treatment is underscored by its inclusion in wound care products especially in the form of antiseptic creams [31]. Additionally, its diverse utility extends beyond wound care, with investigations on its anti-cancer [32] and antioxidant [33] properties, highlighting its versatile potential in various medical contexts.

Considering these factors, this study explored the potential of integrating boric acid into electrospun PLCL fibers, supplemented with EGF, as an advanced wound dressing solution. It was hypothesized that this approach may not only expedite wound healing and reduce susceptibility to infection but also enhance the mechanical properties of the dressings due to PLCL's inherent elasticity. A comprehensive analysis was conducted to determine key factors, including fiber morphology, chemical bonds, swelling capacity, water vapor transmission rate, oxygen permeability, and pH variation in PBS. Additionally, mechanical properties were assessed through tensile tests, while cytocompatibility was evaluated through in vitro fibroblast culture. Furthermore, bacterial adhesion tests involving *E. coli* were performed.

2 Experimental

2.1 Materials

PLCL copolymer with an L-lactide to ε-caprolactone ratio of 85:15 and an inherent viscosity midpoint of 1.6 dl/g (PURASORB PLC 8516, Corbion Purac, Netherlands) was used for fiber production. The solvents were chloroform ($CHCl_3$, purity ≥ 99%, Isolab Gmbh, Germany) and 1,1,1,3,3,3-hexafluoro-2-propanol (HFIP, purity ≥ 99%, Sigma, USA). Boric acid (BA, H_3BO_3, ACS reagent, ≥ 99.5%), sodium chloride (NaCl, ACS reagent, ≥ 99.5%), potassium chloride (KCl, ACS reagent, 99.0–100.5%), disodium hydrogen phosphate (Na_2HPO_4, ACS reagent, ≥ 99.0%), potassium phosphate monobasic (KH_2PO_4, ACS reagent, ≥ 99.0%), and hydrochloric acid (HCl, ACS reagent, 37%) were purchased from Sigma Aldrich, Merck KGaA, Darmstadt, Germany. Dulbecco's modified medium (DMEM) and fetal bovine serum (FBS), penicillin/streptomycin solution were obtained from Gibco (Life Technologies, USA). Human epidermal growth factor (EGF) was procured from Biobasic, Canada. Cell labeling dyes, including FITC-phalloidin (Fluorescein isothiocyanate-labeled phalloidin) and DAPI (4,6-diamidino-2-phenylindole, dihydrochloride), were procured from Abcam, Cambridge, UK. Mueller Hinton Agar and Nutrient Broth No. 3 (Sigma-Aldrich, Merck KGaA, Darmstadt, Germany) was used in bacterial adhesion tests.

2.2 Preparation of Electrospinning Solutions

The PLCL copolymer was dissolved in a 10% (w/v) chloroform using a magnetic stirrer (Isolab Eschau, Germany) at 800 rpm and room temperature for 30 min. To optimize fiber morphology, a solvent blend comprising 80% chloroform and 20% HFIP was also employed. For PLCL solutions containing BA, a mixture of 10% (w/v) PLCL, 80% chloroform, and 20% HFIP by volume was created, followed by the addition of 3–5% (w/v) boric acid with coarse or fine particles. To reduce particle size BA particles ground with an agate mortar and subsequently sieved through a 38 µm stainless steel sieve. The resulting compositions of electrospinning solutions can be listed as:

1. 10% (w/v) PLCL in chloroform
2. 10% (w/v) PLCL in 8:2 (v/v) chloroform/HFIP
3. 10% (w/v) PLCL and 3% (w/v) coarse BA particles in 8:2 (v/v) chloroform/HFIP
4. 10% (w/v) PLCL and 3% (w/v) fine (≤ 38 µm) BA particles in 8:2 (v/v) chloroform/HFIP
5. 10% (w/v) PLCL and 5% (w/v) fine (≤ 38 µm) BA particles in 8:2 (v/v) chloroform/HFIP

2.3 Electrospinning Process

Fiber production was carried out using a desktop electrospinning device (Nanospinner, Inovenso, Istanbul, Turkey) for a duration of 15 min under a voltage range of 8–10 kV, employing a flow rate of 1–1.5 mL/h, and maintaining a distance of 15 cm. The electrospinning processes were conducted at a relative humidity ranging between 50 and 60% and at a typical room temperature of 24 °C. A 21G needle was used as the electrospinning nozzle. Randomly oriented fibers were collected on aluminum foil attached to a metal target. The electrospun fiber patches were maintained at 37 °C for a duration of one week to remove any remaining solvents. The fibrous patches obtained through the electrospinning process of pure PLCL, PLCL containing 3% boric acid (PLCL-3BA), and PLCL containing 5% boric acid (PLCL-5BA) are named accordingly.

2.4 Scanning Electron Microscopy (SEM)

The morphology of the electrospun fibers was investigated using a scanning electron microscope (SEM, Vega 3, Tescan, Brno, Czech Republic). To enhance electrical conductivity, the fibers on the foil were initially coated with gold/palladium (Au/Pd) using a sputter coater (SC7620, Quorum Technologies, Lewes, UK) and were examined at an acceleration voltage of 10 kV. Additionally, fine and coarse BA particles were also subjected to SEM examination. Image analysis was performed using ImageJ (Fiji) software,

developed by the National Institutes of Health (NIH), to measure and analyze the fiber diameters and particle sizes. The mean diameter of the fibers within each electrospun mat was determined by measuring the diameter of 50 randomly selected individual fibers. The size of the particles was also determined similarly.

2.5 Fourier Transform Infrared Spectroscopy (FTIR)

A Fourier transform infrared spectroscope equipped with an integrated attenuated total reflection (ATR) unit (FTIR-ATR, Spectrum 100, PerkinElmer, Norwalk, CT, USA) was utilized to collect the infrared spectra of pure PLCL fibers and fibers containing BA. The analysis was performed with the wavenumber ranging from 650 to 4000 cm^{-1} at a resolution of 1 cm^{-1} and the number of scans was 16.

2.6 Determination of Swelling Capacity

The swelling behavior of the samples was determined using the gravimetric method. Each specimen was immersed in phosphate-buffered saline (PBS, pH = 7.3) maintained at 37 °C within a laboratory oven (MKD-500, Mikrotest, Ankara, Turkey) for various time intervals. At each time point, excess solution was removed from the samples using filter paper, and then their weights were measured using a precision balance (ACE120, Axis, Gdańsk, Poland). The degree of swelling (%) was calculated according to the following equation:

$$Swelling\% = \frac{W_s - W_d}{W_d} \times 100, \quad (1)$$

where W_s represents the weight of the sample in its swollen state after immersion in PBS, and W_d is the weight of the dry sample. The swelling percentage corresponds to the average of three independent tests (n = 3) repeated for each group.

2.7 Determination of pH Change

For the assessment of pH changes induced by the release of BA from the 40 mg samples immersed in a 15 ml PBS solution (n = 3) at the end of each time interval, the pH variations were measured. The possible alteration in pH of PBS over 14 days was also quantified. The resulting values from the control were subtracted and standardized against the measured pH values of the respective sample groups at the specific measurement time point.

2.8 Tensile Test

A uniaxial mechanical testing device (Univert, CellScale Biomaterials Testing, Waterloo, ON, Canada) was utilized to perform tensile tests. Specimens were prepared with dimensions of 40 mm × 10 mm and mounted within the grips to establish a gauge length of 20 mm (n = 4). Tensile tests were conducted at a constant speed of 1 mm/min, employing a 200 N load cell. Data were obtained using software integrated with the mechanical testing device. Young modulus of the specimens was calculated by determining the slope of the stress–strain curve within the linear elastic region.

2.9 Determination of Water Vapor Transmission Rate and Oxygen Permeability

Water vapor transmission rates (WVTR) were assessed following a modified American Society for Testing and Materials (ASTM) E96-90 standard procedure. The test set-up comprised a tightly sealed plastic container, a digital hygrometer, and a saturated magnesium chloride ($MgCl_2$) solution reservoir. The system was situated in a 37 °C incubator with 40 ± 2% relative humidity. A 2.5-cm-diameter specimen was mounted on a plastic cup containing 20 g of dH_2O and placed into the test setup. Water loss through the specimen (n = 3) was determined by monitoring daily weight changes. WVTR was calculated by [34]

$$WVTR\left(\frac{g}{m^2} day^{-1}\right) = \frac{\Delta W}{t \times A}, \quad (2)$$

where ΔW is the mass change in grams, t is the time in days and A is the permeation area of sample in m^2.

For the assessment of oxygen permeability, bottles containing 100 ml of boiled and cooled dH_2O were sealed with samples from each group (n = 3). An open-lid bottle was employed as a control to enable oxygen dissolution in the water. The measurements were carried out for the fiber dressings, along with negative and positive control groups, utilizing a dissolved oxygen meter (HI2004 Edge, Hanna Instruments, United Kingdom) on days 1, 3, and 7. The resultant saturation values were converted to mg/L.

2.9.1 Assessment of In Vitro Cytotoxicity

For in vitro cytotoxicity testing, 3T3 mouse fibroblast cells (NIH/3T3, ATCC CRL-1658) were used. Cells in their 6th passage were cultured in DMEM (high glucose with L-glutamine) supplemented with 10% FBS and 1% penicillin/streptomycin solution at 37 °C. Prior to cytotoxicity tests, the samples were sterilized by immersing in 70% ethanol for 20 min and exposing to UV light for 15 min. Additionally, samples with and without BA were also immersed in human EGF with a weight ratio of 0.1% EGF (in PBS) considering the fiber weight. All groups, including those with samples soaked in the EGF solution, were cut to a diameter of 10 mm, and placed into 24-well cell culture plates. A cell suspension was added to each well at a density of 10,000

cells/cm^2. A control group was established using a tissue culture plate (TCP). Subsequently, the cells were allowed to adhere to the fibers by incubating them at 37 °C and 5% CO_2 for 30 min. Following this, 500 µl of complete culture media was added to each well, and the plates were then incubated in an atmosphere of 5% CO_2 at 37 °C for 24 h. Following this, PrestoBlue™ cell viability reagent was introduced into the cell culture plates at 1, 3, and 7 days of incubation. After allowing the reagent to incubate with the cells for a 4 h period, the absorbance was measured using a spectrophotometer at wavelengths of 570 nm and 600 nm. Absorbance data underwent analysis for normality and homogeneity of variance through the application of the Shapiro–Wilk and Levene tests. Subsequently, one-way ANOVA followed by Bonferroni's post-hoc comparisons tests were employed. Statistics with a value of $p < 0.05$ were considered significant.

2.9.2 Assessment of Cell Morphology with SEM and Fluorescent Microscopy

At the end of the 7th day of incubation, the cells were treated with 2.5% glutaraldehyde at room temperature for fixation. Afterward, they were dehydrated by immersing sequentially in 50%, 70%, 80%, 96% and absolute alcohol series for 30 min each and then dried using hexamethylsiloxane (HMDS). Before imaging the cell-seeded samples using a high-resolution field emission scanning electron microscopy (FESEM, Hitachi High-Tech, Tokyo, Japan), a sputter coater (EM ACE600, Leica Microsystems, Wetzlar, Germany) was used to provide a thin coating (5 nm) of gold.

For fluorescent microscopy visualization of the cells, FITC-phalloidin and DAPI cell labeling dyes were employed. Initially, FITC-phalloidin was diluted in PBS at a 1/1000 ratio following the manufacturer's protocol, with the addition of 0.1% bovine serum albumin (BSA). After application to the fixed cells, it was left for 1 h and then washed with PBS. DAPI, obtained as a 10 mM solution, was added to the wells at a final concentration of 2.5 µM and incubated at room temperature for 30 min. Afterward, DAPI was removed from the cells, which were then washed twice with PBS. Finally, the cells were imaged using a fluorescence microscope (DMi8 S, Leica Microsystems, Wetzlar, Germany).

2.9.3 Determination of Bacterial Adhesion

Gram-negative bacteria, *E. coli* (ATCC® BAA-2471™, USA), were used as the model bacterial strain to assess adhesion. Sterile samples of PLCL, PLCL-3BA and PLCL5BA were cut into circular shapes with a 1 cm diameter. Mueller–Hinton agar was prepared in distilled water at a concentration of 3.8%. Bacteria were suspended in Nutrient Broth No. 3 solution (13 g/L in dH_2O) and vortexed for 1 min. Subsequently, the bacterial inoculums were spread over the Muller–Hinton agar plates using sterile cotton swabs. The samples were placed on Petri dishes and incubated at 37 °C for 24 h. After incubation, the samples were washed with sterile PBS solution to remove any unattached bacteria. The samples were then fixed in a paraformaldehyde in PBS solution (2.5% w/v) for 30 min for bacterial fixation. For dehydration, the samples were treated with 50%, 70%, 80%, 96% and absolute ethanol for 30 min in each. To observe the bacteria adhering to the surfaces of the samples, the surfaces were coated with a 5 nm layer of gold/palladium (Au/Pd) using a sputter coater (EM ACE600, Leica Microsystems, Wetzlar, Germany) before being examined with a scanning electron microscope (FESEM, Hitachi High-Tech, Tokyo, Japan).

3 Results and Discussion

3.1 Fiber Production and Morphology

Electrospinning is a promising method for producing fibrous materials with a wide range of applications in fields such as wound care and tissue engineering. However, the process needs careful optimization to achieve the desired properties. The SEM micrographs given in Fig. 1 display the morphological characteristics of the electrospun PLCL fibers produced in the optimization of fiber morphology, shedding light on the impact of various electrospinning parameters, including solvent composition, voltage, distance, and flow rate.

The fibers produced with 10% PLCL in chloroform, under the electrospinning conditions of 10 kV voltage, 15 cm distance, and 1 mL/h flow rate, exhibited a significant variation in fiber diameter, with both thin and thick fibers evident, as shown in Fig. 1a. ImageJ analysis revealed that the diameters of randomly selected fibers ranged from 0.125 to 10.925 µm, with a mean diameter of 2.261 ± 3.011 µm. The fiber morphology appeared to be straight (non-branched) but highly porous in the thick fibers. As shown in Fig. 1b**,** the decrease in voltage from 10 to 8 kV had no significant impact on fiber diameter and porous morphology. The mean diameter was calculated as 2.851 ± 3.275 µm. It is known that porous electrospun fibers offer large specific surface area for applications like drug delivery but can significantly reduce tensile strength due to the void spaces within the structure. In addition, fibers with a smaller diameter have a higher tensile strength [35]. The primary mechanism responsible for the creation of porous fibers is suggested to the phase separation [36]. When employing solvents with higher volatility, regions rich in solvent begin to develop during the electrospinning process, ultimately evolving into pores. As demonstrated previously, substituting solvents,

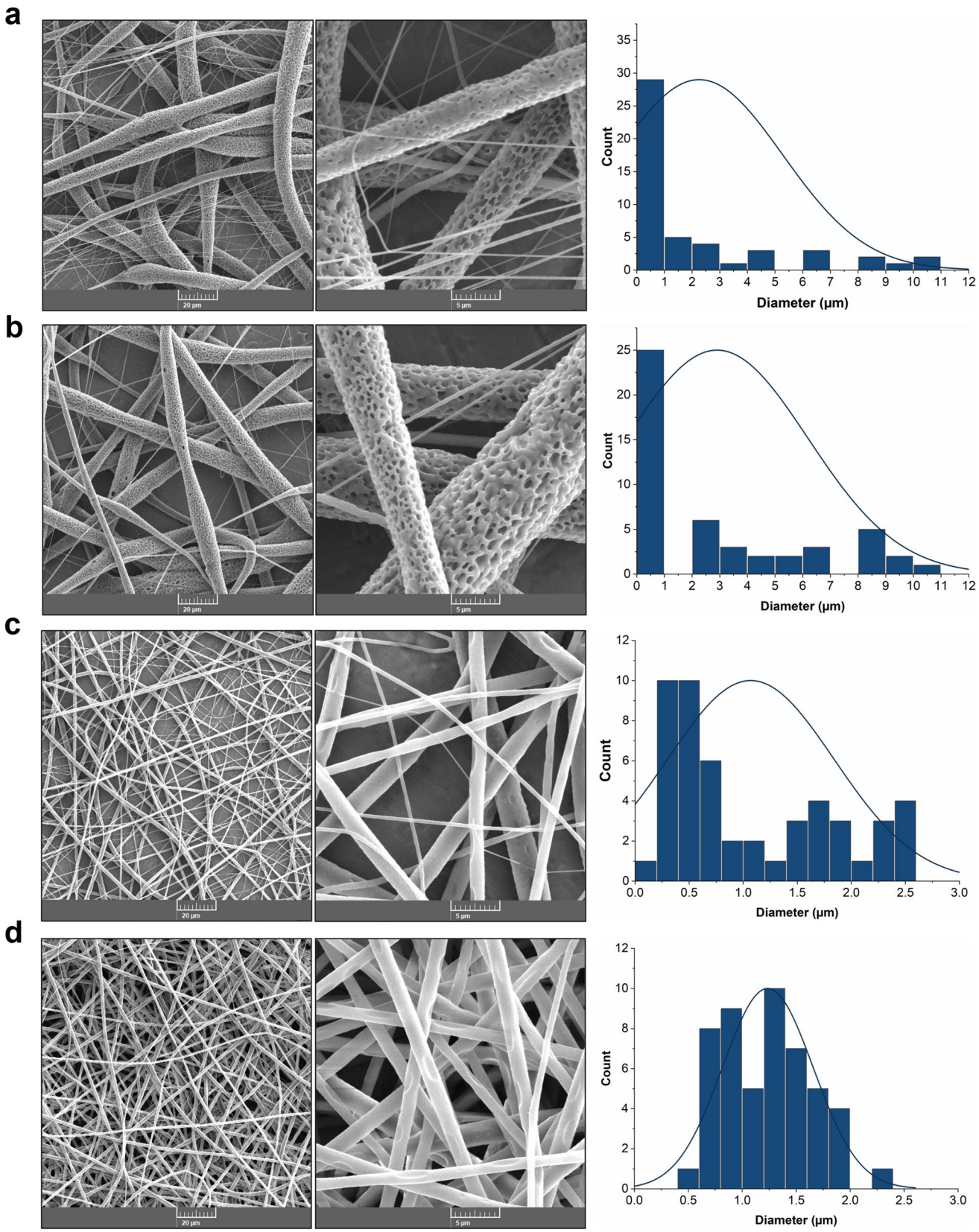
a
20 μm
5 μm
Count
Diameter (μm)
b
20 μm
5 μm
Count
Diameter (μm)
c
20 μm
5 μm
Count
Diameter (μm)
d
20 μm
5 μm
Count
Diameter (μm)

◂**Fig. 1** SEM micrographs and fiber diameters of pure PLCL fibers produced using various electrospinning parameters, including solvent(s), voltage, distance, and flow rate as listed in the given order at two different magnifications: **a** chloroform, 10 kV, 15 cm, and 1 mL/h, **b** chloroform, 8 kV, 15 cm, and 1 mL/h, **c** 8:2 (v/v) chloroform/HFIP, 8 kV, 15 cm, and 1 mL/h, **d** 8:2 (v/v) chloroform/HFIP, 8 kV, 15 cm, and 1.5 mL/h. Scale bars: 20 µm for the left micrographs and 5 µm for the right micrographs in each row

such as dichloromethane, with solvents having lower vapor pressure, like chloroform, can substantially diminish the likelihood of pore formation [37]. In this study, a secondary solvent, HFIP, was introduced into the PLCL solution. HFIP (21.2 kPa) exhibits lower vapor pressure compared to chloroform (26.2 kPa), indicating its lower volatility in comparison to chloroform [38]. As evident in Fig. 1c and d, the addition of HFIP to the PLCL solution resulted in a significant change in fiber morphology. Specifically, employing a mixture of 8:2 (v/v) chloroform/HFIP, along with 8 kV voltage, 15 cm distance, and a flow rate of 1 mL/h, resulted in a notable reduction in fiber diameter, yielding relatively uniform fiber diameters (Fig. 1c). ImageJ analysis revealed that the diameters of randomly selected fibers reduced to a mean diameter of 1.070 ± 0.772 µm. The relationship between flow rate and fiber diameter was previously reported to be influenced by the distance from the source, however, increasing flow rate is generally expected to lead to an increase in fiber diameter [39]. In this study, maintaining other parameters constant and increasing the flow rate from 1 mL/h to 1.5 mL/h resulted in the generation of fibers with more consistent diameters compared to those produced under different parameter conditions (see Fig. 1d). However, ImageJ analysis of 50 randomly selected fibers in the left pane of Fig. 1d still indicated the presence of both micro and nanofibers with an average diameter of 1.236 ± 0.468 µm, demonstrating a reduced standard deviation.

SEM micrograph of boric acid particles that underwent grinding and were subsequently sieved through a 38 µm pore size mesh is displayed in Fig. 2a. The particle sizes were measured using ImageJ, and the resulting histogram is shown in Fig. 2b. Similarly, in Fig. 2c, SEM micrograph of boric acid particles that were used in their as-purchased (coarse) state are presented, and the corresponding particle size histogram is provided in Fig. 2d.

The optimization of electrospinning for PLCL fibers containing 3–5% boric acid (PLCL-3BA and PLCL-5BA) has also been carried out during the electrospinning process. SEM observations revealed that all PLCL fibers with incorporated boric acid displayed uniform fiber diameters and boric acid particles did not aggregate across the fiber area. The SEM micrograph of the fibers fabricated using electrospinning parameters of 10 kV, 15 cm, and 1.5 mL/h, from a PLCL solution comprising 3% coarse boric acid particles is presented Fig. 3a**,** with an average diameter of 1.280 ± 0.414 µm. Interestingly, the PLCL fibers were observed to encase the boric acid particles, forming an envelope around them. The SEM micrograph inset, presented in Fig. 3a, provides a visual representation of the formation of a fiber node around one of the coarse particles. Similarly, electrospun PLCL fibers containing fine boric acid particles in weight percentages of 3% (Fig. 3b and c) and 5% (Fig. 3d) were likewise observed to accumulate around the particles. In the case of fine particles, tight envelopment did not occur; instead, the fibers were drawn around the particles, resulting in a unique morphology, with some particles visible beneath the PLCL fibers in SEM micrographs. The average diameters for the fibers in Fig. 3b, 3c, and 3d are 1.176 ± 0.455 µm, 1.185 ± 0.539 µm, and 1.110 ± 0.421 µm, respectively. The incorporation of boric acid in the electrospinning of polyacrylonitrile (PAN) fibers was previously investigated as a triboelectric contact layer to enhance the power production performance of PAN [40]. The study reported a reduction in fiber diameter and a wider size distribution, attributed to the interference of boric acid ions with the polymer. The absence of a similar trend in size reduction and widened diameter distribution in this study suggests that the dissolved or particulate forms of boric acid in the system may contribute differently to the electrospinning process.

Selvakumar et al. investigated the incorporation of boric acid in the particulate form as an additive into a synthetic polymer solution, followed by the utilization of the electrospinning technique to create fibers [41]. In this particular study, nano-sized boric acid was introduced into a polyamide solution at a maximum concentration of 0.05 wt %, primarily aimed at the development of flame-retardant textiles. However, no distinct fiber morphology, such as the aggregation of polyamide fibers around boric acid, has been reported. The interaction between PLCL fibers and boric acid particles observed in the present study can be attributed to a combination of several influential factors, including electrostatic forces, rheological behavior, and the concentration and size of the boric acid particles. Regarding size, fine particles tend to be entrained by the polymer jet due to their lower mass, while coarser particles become enveloped by the surrounding polymer solution and may reach the collector as part of a droplet. Consequently, the use of finely structured particles in the production of PLCL-BA composite fibers was pursued after these optimizations for further characterizations.

3.2 Fourier Transform Infrared Spectroscopy (FTIR) Analysis

To identify the functional groups, PLCL, PLCL-3BA and PLCL-5BA fibers were characterized using FTIR-ATR spectrometry (see Fig. 4).

The primary infrared (IR) bands of PLCL, as depicted in Fig. 4a, were assigned as follows: 2993 and 2944 cm^{-1}

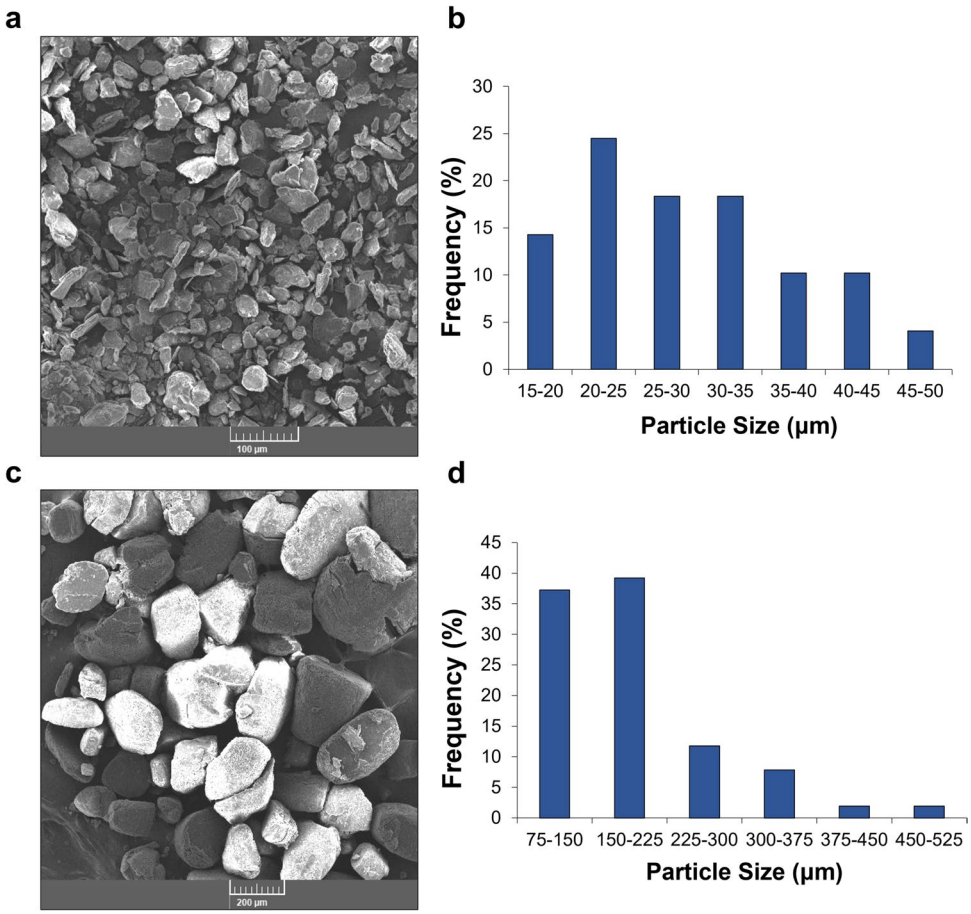

Fig. 2 **a** SEM micrograph of fine BA particles (Scale bar: 100 µm), **b** size distribution graph of fine BA particles depicted in a, **c** SEM micrograph of coarse BA particles (Scale bar: 200 µm), and **d** size distribution graph of coarse BA particles depicted in **c**

(C–H stretching) [42–44], 1751 cm^{-1} (C = O stretching) [45], 1453 cm^{-1} (CH_3 bending) and 1382 cm^{-1} (CH_3 symmetric deformation) [46], 1182, 1129, 1086 and 1044 cm^{-1} (–C–O–C group) [42, 47–49], 870 cm^{-1} (C–COO stretching) and 756 cm^{-1} (C = O in-plane bending) [50]. In the IR spectra of PLCL-5BA, the band at 3193 cm^{-1} (O–H stretching) was attributed to boric acid [51]. Another new band appearing at 2259 cm^{-1} was assigned to B–O stretching [52]. Additional boric acid-related bands were expected to appear as follows: O–H stretching at 3200 cm^{-1}, B–O stretching at 1450 cm^{-1}, and B–O–H bending vibration at 1190 cm^{-1} [53]. However, the band at 1190 cm^{-1} overlapped with PLCL-related IR bands. Furthermore, due to the overlap between the 1450 cm^{-1} and the 1453 cm^{-1} bands, the intensity of the former increased in the fibers containing boric acid. A new band originating from the inclusion of boric acid, specifically at 801 cm^{-1}, was assigned to assigned to B–OH out of plane bending [54]. Moreover, the bands associated with boric acid were observed to be more distinct in the spectrum of PLCL-5BA compared to that of PLCL-3BA.

3.3 Physical Properties: Swelling Capacity, pH Change in PBS Solutions, Oxygen Permeability and Water Vapor Transmission Rate (WVTR)

Swelling capacity of fibers were determined in PBS (pH 7.3) at 37 °C and are depicted in Fig. 5a. PLCL fibers containing boric acid exhibited reduced swelling rates compared to pure PLCL samples, with the reduction in swelling rate becoming more pronounced as the boric acid content increased. This decline in weight gain through water absorption in the boric acid-containing fibers was attributed to the decrease in weight loss associated with the release of boric acid. After 24 h, the pure PLCL samples exhibited the highest swelling rate at 151 ± 10.3%. This rate significantly surpasses the swelling rates reported by Wang et al. for four commercial wound dressings, including DuoDERM®, HydroColl® and Tegaderm™, which all showed swelling rates below 10% in distilled water at 25 °C for 4 h, indicating minimal water absorption [55].

Intact skin maintains its natural acidity through a pH level spanning from 4 to 6, which is a result of organic acid secretions by keratinocytes in the epidermis [56]. When the skin

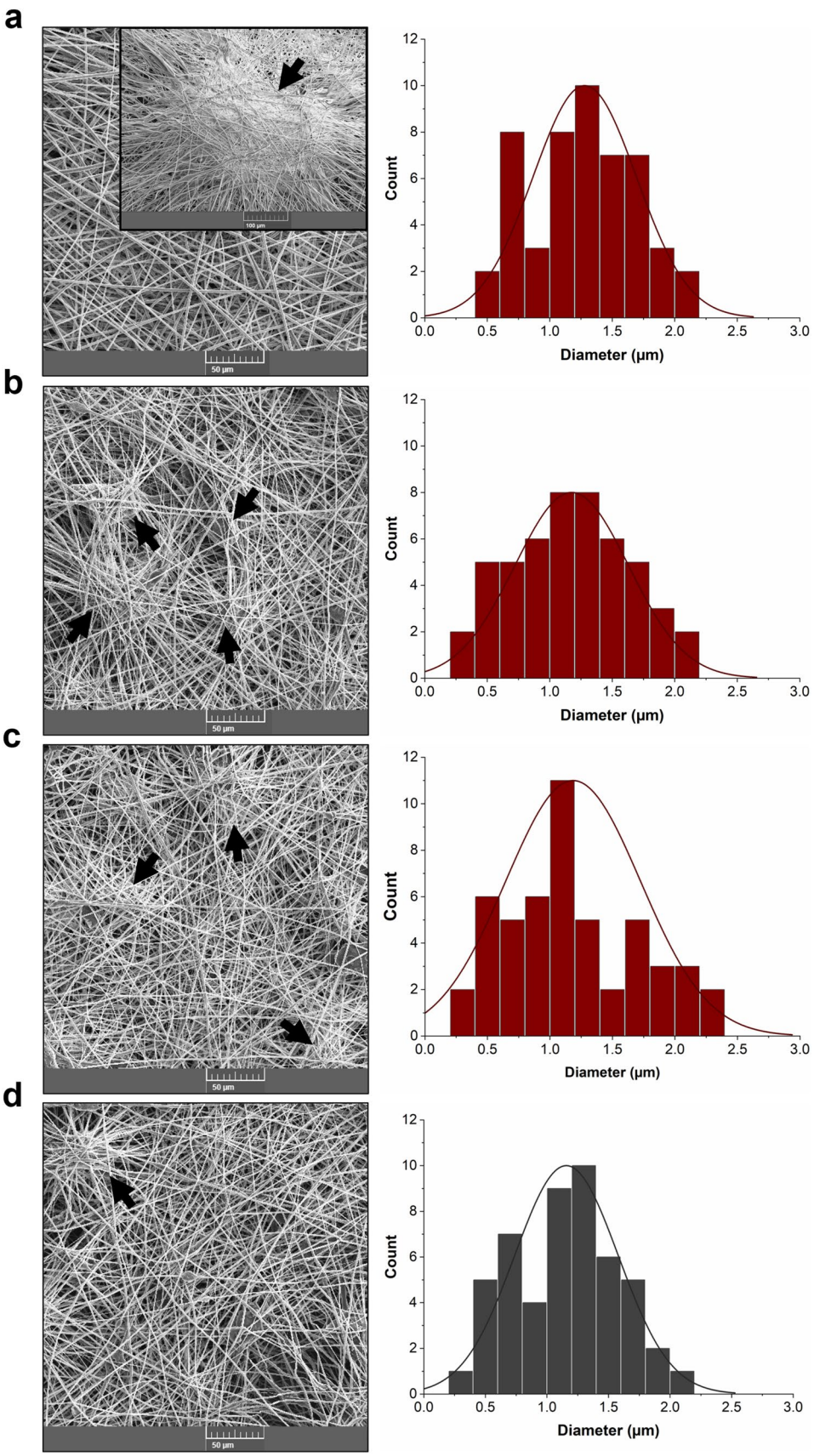

Fig. 3 SEM micrographs and fiber diameters of PLCL-3BA and PLCL-5BA fibers produced using various electrospinning parameters. BA amount, solvent(s), voltage, distance, and flow rate are as follows: **a** 3% coarse BA, 8:2 (v/v) chloroform/HFIP, 10 kV, 15 cm, and 1.5 mL/h (inset shows a node formed by PLCL fibers around a coarse BA particle), **b** 3% fine BA, 8:2 (v/v) chloroform/HFIP, 8 kV, 15 cm, and 1.5 mL/h, **c** 3% fine BA, 8:2 (v/v) chloroform/HFIP, 10 kV, 15 cm, and 1.5 mL/h, and **d** 5% fine BA, 8:2 (v/v) chloroform/HFIP, 10 kV, 15 cm, and 1.5 mL/h (Scale bars: a, b, c and d 50 µm and insert in a 100 µm). Arrows indicate the nodes formed due to the presence of BA particles

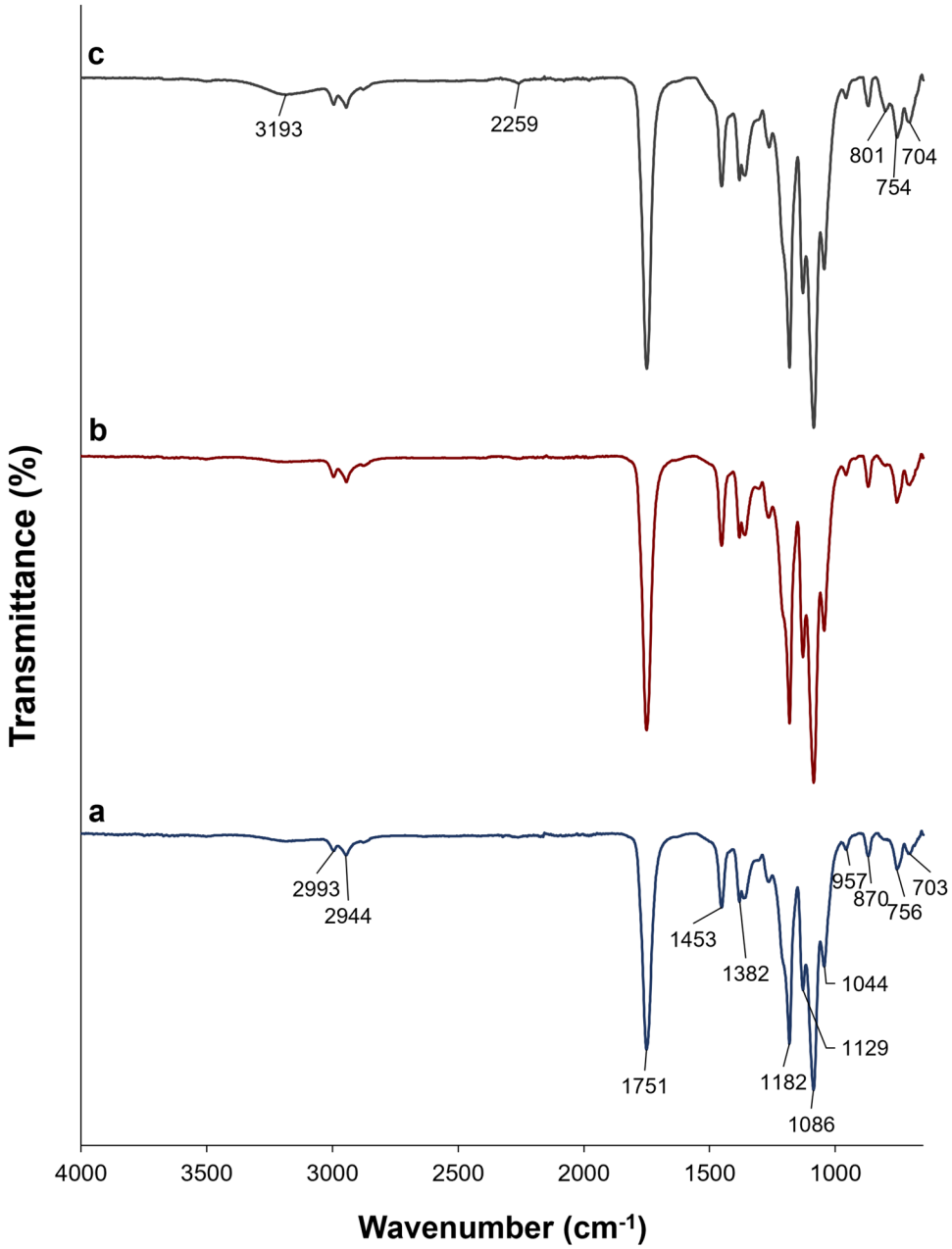

Fig. 4 FTIR spectra of the fibers: **a** PLCL, **b** PLCL-3BA, and **c** PLCL-5BA

is damaged, the pH of the wound surface rises as a result of fluid leaking from microvessels and approaches the body's physiological pH of 7.4, making the wound more vulnerable to bacterial infections [57]. The pH value rises, often between pH 7.5 and 8.9, which produces inflammation and slows down the healing process. The effects of pH on the attachment, proliferation, and migration of keratinocytes and fibroblasts were previously investigated in vitro and ex vivo skin models and it was reported that the optimal pH for both keratinocyte and fibroblast proliferation is between pH 7.2 and 8.3, while low pH stimulated keratinocyte differentiation [58]. In this study, the objective was to moderately adjust the pH towards the slightly acidic range, while ensuring that it did not excessively influence fibroblast adhesion and proliferation behaviors. Therefore, pH variations resulting from boric acid release and the hydrolytic degradation of PLCL in an aqueous environment were monitored, and the results are displayed in Fig. 5b. The results showed that the immersion of PLCL-5BA (40 mg) in PBS (15 ml) resulted in a decrease in pH from 7.30 to 7.13 ± 0.03. Various acids have been previously incorporated into wound dressings to take advantage of their properties, including antibacterial and anti-inflammatory effects. The examples of these acids include ferulic acid [59], tannic acid [60], and salicylic acid [61] and gallic acid [62]. However, there has been no emphasis on monitoring and controlling pH changes within

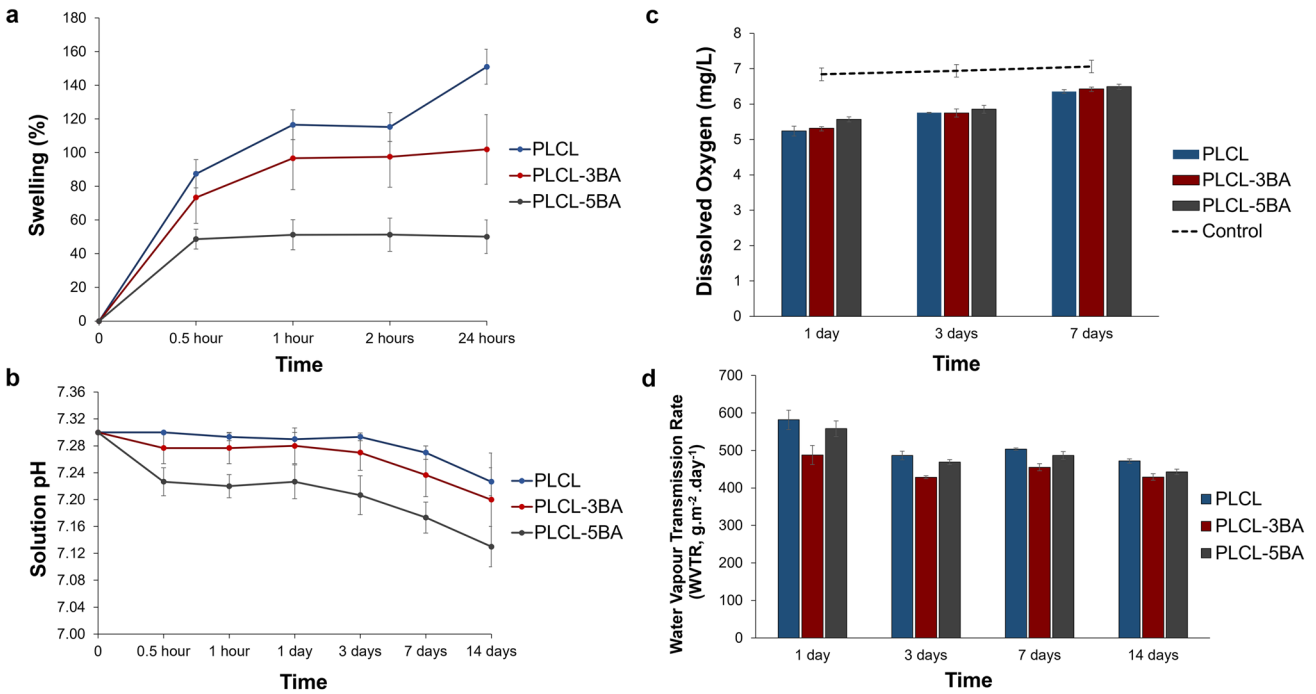

Fig. 5 **a** Swelling capacity of the PLCL, PLCL-3BA and PLCL-5BA fibers in PBS at 37 °C, **b** the pH change of PBS solutions in which PLCL, PLCL-3BA, and PLCL-5BA fibers were immersed for 14 days, **c** the amount of dissolved oxygen in water, indicating the oxygen permeability of PLCL, PLCL-3BA and PLCL-5BA fibers and control (open-lid bottle), and **d** water vapor transmission rates (WVTR) of the PLCL, PLCL-3BA and PLCL-5BA fibers over 14 days. Error bars represent the standard deviation (n = 3).

the wound environment in these attempts. In one of the few studies conducted for this purpose, an agar-citric acid bilayer wound dressing was produced, and the pH changes in wound simulation fluid (WSF) were monitored [63]. A 1cm^2 agar dressing containing 7.5% citric acid was found to lower the pH of 1 mL WSF from 8.5 to 6.5 and it was concluded that the dressings would be able to modulate the wound exudate to around pH 6–6.5. However, it is important to note that non-standardized experimental conditions create challenges for making direct comparisons between these studies.

Oxygen plays a pivotal role in the wound healing process, as it is essential for various healing mechanisms, including collagen deposition, epithelialization, angiogenesis, and infection resistance [64]. However, impaired oxygen supply to the wound area can obstruct these physiological healing processes. The oxygen permeability of the fibers was assessed by measuring percent saturation with an oxygen meter, as depicted in Fig. 5c, and these values were later converted to mg/L. When comparing the results to the open control, which recorded a dissolved oxygen value of 7.06 ± 0.18 mg/L, the PLCL-5BA fibers showed a slightly lower but still substantial dissolved oxygen concentration of 6.49 ± 0.07 mg/L on the seventh day. Tehrani et al. developed a specialized wound dressing for controlled oxygen release through H_2O_2-loaded polylactic acid (PLA) microparticles, demonstrating an initial burst release on the first day, followed by stabilization at around 8 mg/L of dissolved oxygen from the third day [65].

In healthy skin, the water vapor transmission rate (WVTR) typically measures around 204 g/m^{2}day, but in the case of damaged or injured skin, this rate can significantly increase, reaching levels as high as 5138 g/m^{2}day [66, 67]. Many publications reporting WVTR of wound dressings lack clarity regarding the methods used, making it difficult to compare WVTR values between studies unless standardized methods are employed [68]. However, it is known that a high WVTR can lead to rapid water loss, potentially causing wound dehydration and dressing adhesion issues, while a low WVTR may result in exudate retention, back pressure, maceration of surrounding healthy tissue, and patient discomfort [69]. The recommended WVTR range for wound dressings is typically half of that observed in granulating wounds, around 2000–2500 g/m^{2}day [70], but in practice, many widely used commercially available dressings, like Comfeel®, Dermiflex®, Tegaderm™ and OpSite®, do not conform to this range, having values of 285, 76, 491, and 792 g/m^{2}day, respectively. WVTRs of the PLCL and boric acid added PLCL fibers produced in this study over 14 days are presented in the graph in Fig. 5d. The WVTR of PLCL-5BA fibers were 557 ± 20.9 g/m^{2}day at 24 h. The WVTR of all fibers are not only consistent with commercial products but also comparable to findings in the literature. For

example, wound dressings composed of electrospun PU membranes with silver nanoparticles exhibited a WVTR of 220 g/m^{2}day [71], while a silver nanoparticle-impregnated bacterial cellulose matrix demonstrated a WVTR of approximately 400 g/m^{2}day [72].

3.4 Tensile Test

The mechanical properties play a crucial role in the suitability of wound dressings, requiring both adequate tensile strength and flexibility to endure handling and replacement [73]. The tensile properties of the wound dressings were evaluated and the representative stress–strain graphs, as well as the maximum tensile stresses, are given in Fig. 6.

The mechanical properties of all fibers were found to be within an appropriate range for utilization in wound dressing applications. Previous literature has indicated that human skin can exhibit a wide range of values for tensile strength (1–32 MPa) and elongation at break (17–207%) [74]. It was noted that pure PLCL fiber samples had the lowest tensile strength and the incorporation of boric acid particles into the PLCL fiber structure was observed to enhance tensile strength and markedly increase elongation at break values. PLCL-3BA and PLCL-5BA exhibited comparable mean maximum stress values at 11.25 ± 0.90 MPa and 11.31 ± 0.82 MPa, respectively, in contrast to pure PLCL, which reached 6.92 ± 2.08 MPa. Young's modulus values were also determined to characterize the fibers' resistance to elastic deformation under tensile load. The obtained values are as follows: 190.53 ± 64.80 MPa for PLCL, 191.97 ± 51.33 MPa for PLCL-3BA, and 224.74 ± 91.66 MPa for PLCL-5BA. Additionally, during the tensile test, all pure PLCL samples ruptured, whereas PLCL fiber samples with boric acid content did not break completely within the test limits. In line with these findings, a previous study has demonstrated that the incorporation of hydroxyapatite and ZnO particles enhances both the tensile strength and Young's modulus of electrospun PCL fibers [75]. The incorporation of halloysite, a nanoclay mineral, into electrospun chitosan/polyethylene-oxide (PEO) fibers also resulted in an improvement in both tensile strength and Young's modulus, up to a concentration of 5wt% [76]. Beyond this threshold, a decline in these mechanical properties was observed. Lang et al. observed a reduction in tensile stress and elongation in electrospun nanofibrous wound dressings composed of poly(arylene sulfide sulfone) (PASS) as the ZnO particle content increased [77]. Specifically, the PASS fibers with 1% ZnO exhibited a tensile stress of 2.47 MPa and a break extension of 6.81%, while the PASS fibers with 2% ZnO had a tensile stress of 1.98 MPa and a break extension of 4.24%. This trend was attributed to the formation of defects caused by the ZnO nanoparticles, resulting in adverse effects on the mechanical properties of the films. In this study, the addition of up to 5wt% boric acid resulted in improved mechanical properties falling within the range observed in skin tissue, suggesting that this concentration of boric acid contributes to enhanced fiber characteristics compatible with skin tissue.

3.5 In Vitro Fibroblast Proliferation and Morphology

The cytocompatibility of the wound dressings was evaluated using 3T3 mouse fibroblast cells. The absorbance readings in the PrestoBlue assay of PLCL, PLCL-3BA, and PLCL-5BA, along with the EGF solution-treated groups

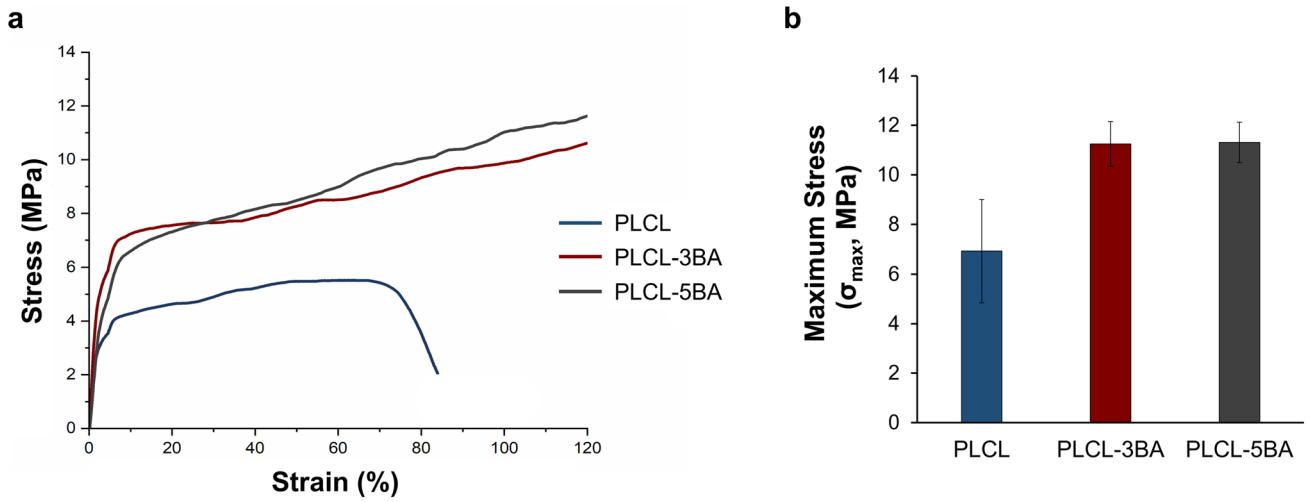

Fig. 6 **a** Representative tensile stress–strain curves of the PLCL, PLCL-3BA and PLCL-5BA fibers, **b** average maximum tensile stress (error bars represent standard deviation, n = 4).

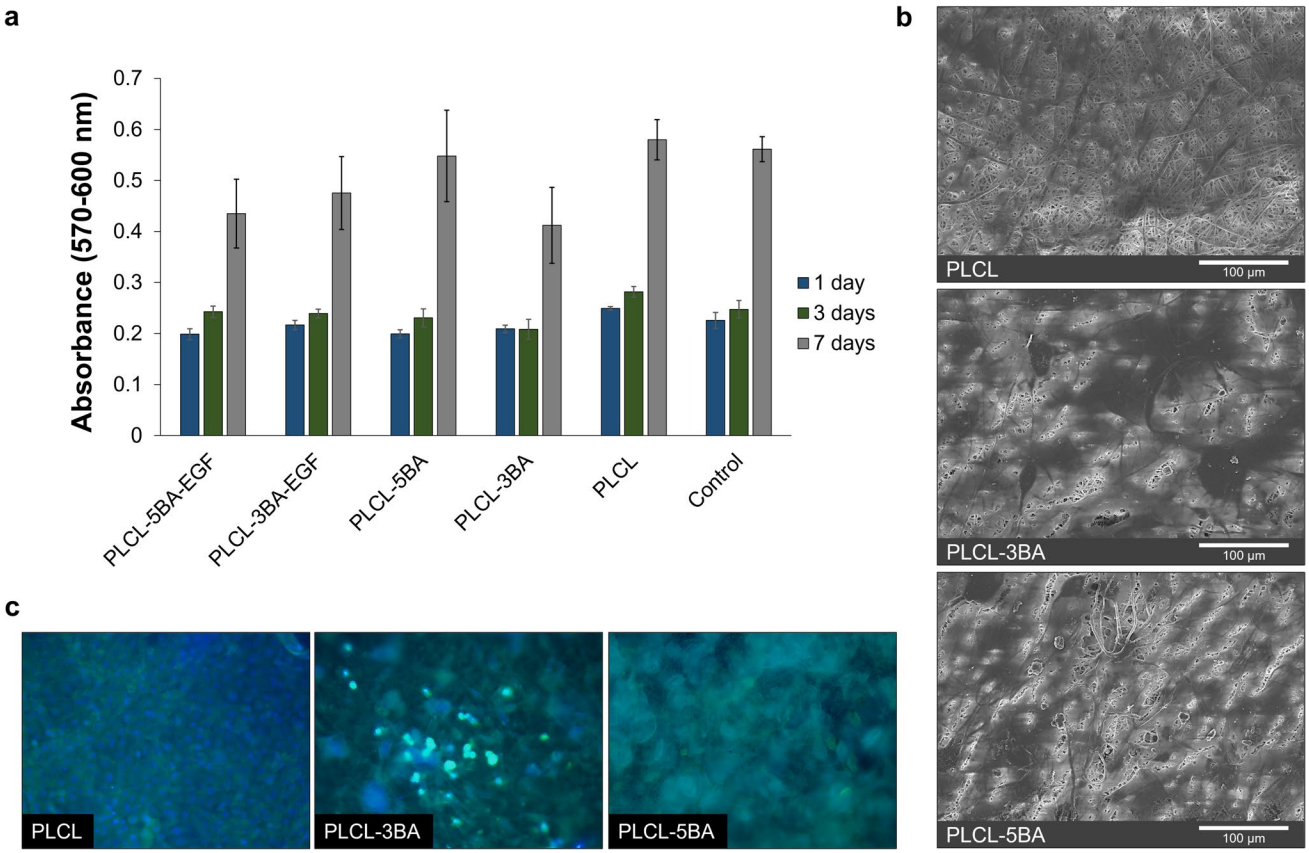

Fig. 7 **a** Fibroblast cell proliferation on various fibers assessed using the PrestoBlue assay over a 7-day period. Data (n = 4) is depicted as the mean ± standard error of the mean for absorbance readings at 570 nm and 600 nm wavelengths, **b** SEM micrographs of fibroblast cells after 7 days of incubation on different fibers (scale bars: 100 µm), and **c** fluorescence microscopy images of fibroblast cells stained with FITC-phalloidin and DAPI after 7 days of incubation on different fibers.

(PLCL-3BA-EGF and PLCL-5BA-EGF), are presented in Fig. 7a. Based on the PrestoBlue assay results, a slight reduction in cell proliferation rate was observed for PLCL-3BA on the 7th day, although it was not statistically significant compared to the control. Overall, despite observed trends, one-way ANOVA and Bonferroni post hoc analysis revealed no statistically significant differences for any of the test groups at any time point compared to the control (cells on tissue culture plate). This suggests that the boric acid containing fibers exhibit comparable performance to the tissue culture plate in terms of supporting cell proliferation, emphasizing their potential as a suitable substrate for cell growth.

It was previously shown that EGF loaded fibrous membranes can be prepared by dispersing EGF solution in polymer solution just prior to electrospinning [78]. However, one crucial consideration is to maintain the stability of EGF within the wound dressing [79]. In this study, to deliver EGF without compromising its biological activity, the wound dressings were treated with EGF solution just before the cell culture experiments. However, no differences were observed between the groups seeded on EGF-treated PLCL fibers and non-EGF-treated PLCL fibers, regardless of the presence of boric acid. Similarly, a wound dressing comprising a hyaluronic acid and collagen sponge with or without EGF was prepared, and it was reported that there was no significant difference between the two groups, with or without EGF, in terms of fibroblast cell viability after 7 days of cultivation [80]. However, the presence of EGF in the sponges significantly increased the release of vascular endothelial growth factor (VEGF) and hepatocyte growth factor (HGF) from the fibroblasts. In this study, the limited impact of EGF on cell proliferation also suggests that, despite being adsorbed onto the surface, EGF tends to be washed away with the discarded cell culture media in vitro due to the absence of a chemical bond with the fibers. However, in vivo, the interaction of EGF with the wound environment may differ, requiring further investigations for a comprehensive understanding of EGF dynamics in wound dressings.

For the assessment of fibroblast cell adhesion and morphology on PLCL fibers with boric acid particles, SEM and fluorescent microscopy analyses were performed. The

SEM micrographs and fluorescence microscopy images of fibroblast cells stained with FITC-phalloidin and DAPI after 7 days of incubation on various fibers are presented in Fig. 7b and Fig. 7c, respectively. SEM images indicate that fibroblast cells adhered and spread effectively on the surface of all groups. Notably, it was evident that cells could readily adhere, spread around, and even attach to boric acid particles that are clearly visible on the surface of PLCL-5BA in Fig. 7b. Fluorescence microscopy observations of cells cultured on PLCL-3BA and PLCL-5BA further corroborated the presence of a dense cell population.

3.6 Bacterial Attachment

Bacterial attachment, essential for biofilm formation, can disrupt wound healing and lead to antibiotic resistance, making it crucial to assess how wound dressing materials influence bacterial attachment [81]. Considering that electrospun PLCL fibers provide an appropriate surface for fibroblast cell attachment, it is reasonable to assume they may also offer high surface area for bacterial cells to adhere. Consequently, this study examined the incorporation of boric acid up to a concentration of 5% in the PLCL electrospinning solution. In particular, boric acid is regarded as safe in healthcare products within specified limits, typically up to 5% in talc, 0.5% in oral hygiene products, and 3% in other items, based on their intended application [31]. Examination of bacterial adhesion using SEM (Fig. 8) confirmed a significant reduction in *E. coli* attachment to both PLCL-3BA and PLCL-5BA, as compared to PLCL fibers. Closely adhered *E. coli* colonies were observed on pure PLCL fibers, while instances of bacterial presence on PLCL-3BA and PLCL-5BA were notably rare and scattered. A previous study on the antimicrobial polyurethane coatings incorporating boric acid derivatives, also confirmed that the coatings exhibit biocidal properties against *E. coli*, *S. aureus*, *P. aeruginosa*, and *K. pneumonia*, although it was noted that the precise mechanism of boric acid's antibacterial action remains hypothetical [82]. However, it was shown to inhibit both gram-positive and gram-negative bacteria, especially *E. coli* and *S. aureus*, through cell wall lysis [83]. The potential mechanisms underlying the broad antimicrobial effects of boron-containing compounds, including boric acid, were attributed to their interaction with amino acid residues (serine, threonine, tyrosine, etc.), and also their contribution to the disruption of synthetic cell-wall processes [84]. This study focused on evaluating the attachment of *E. coli* and further investigations involving gram-positive bacteria are necessary for a comprehensive understanding of the antimicrobial potential of the electrospun fibers.

Moreover, Fig. 8 reveals the signs of degradation were also observed in the SEM micrographs of the electrospun fibers here; however, it is important to consider that these findings may also be attributed to artifacts resulting from the sample preparation for SEM analysis.

4 Conclusions

In this study, the potential of incorporating boric acid into PLCL-fiber-based wound dressings to create versatile solutions for superficial, low-exuding wounds, including partial-thickness burns was investigated. The research revealed that electrospun PLCL fibers possess a three-dimensional, open porous structure with significant alterations in fiber morphology which is optimized during electrospinning. The electrospun fibers exhibited a nano to microscale range. Specifically, the average fiber diameter of PLCL-5BA was measured at 1.110 ± 0.421 µm. The presence of boric acid in the fiber structure was confirmed through FTIR spectroscopy. Boric acid-added fibers demonstrated improved mechanical properties, with higher tensile strength (11.31 ± 0.82 MPa for PLCL-5BA) and strain at break compared to boric acid-free fibers (6.92 ± 2.08 MPa for PLCL). Despite a higher weight gain in pure PLCL fibers during the swelling test in PBS, all boric acid-added fibers, even at a 5% concentration of boric acid, exhibited a good swelling capacity. These results suggest the potential suitability of boric acid-added

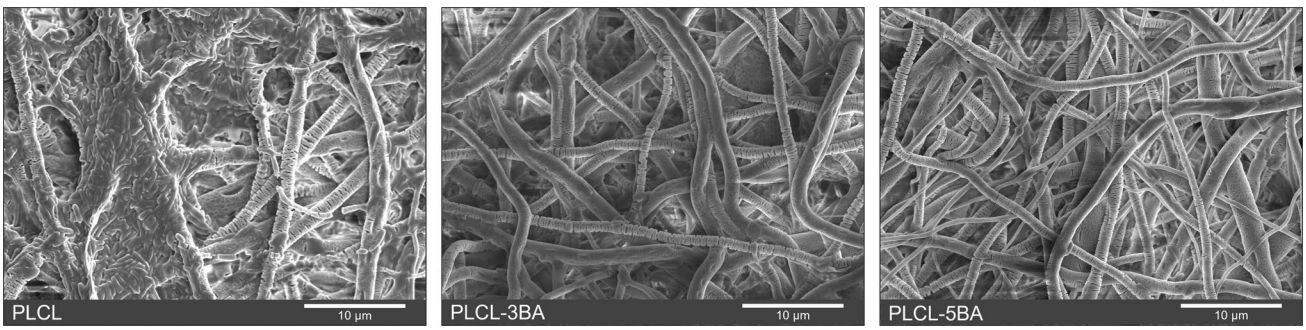

Fig. 8 SEM micrographs of *E. coli* attached to PLCL, PLCL-3BA and PLCL-5BA fibers

dressings for exudate management in low to moderately exuding wounds. The pH variation study confirmed that PLCL-5BA fibers did not result in a dramatic decrease in the pH of the PBS solution (from 7.30 to 7.13 ± 0.03), though it was considered sufficient to lower the pH at the wound site. In addition, the water vapor permeability test revealed that boric acid-containing fibers permit efficient moisture transfer, which could support wound healing. The cell culture experiments, where EGF-treated and untreated PLCL fibers with and without boric acid were evaluated, demonstrated that the fibers serve as a good substrate for fibroblast cell attachment and proliferation. Moreover, a reduction in *E. coli* bacterial attachment and proliferation on boric acid-added fibers was demonstrated, signifying their potential as antibacterial wound dressings. Investigations with higher concentrations of boric acid are needed to enhance its antimicrobial activity, and in vivo evaluations are imperative to validate the clinical potential of these wound dressings. Future assessments, including thermal analysis techniques, may offer valuable insights into the thermal properties, stability, and phase transitions of the fabricated materials, contributing to a more comprehensive understanding of their potential applications.

Acknowledgements This study was conducted at the Experimental Medicine Research and Application Center at the University of Health Sciences, Turkey. The authors would like to express their appreciation to Dr. Ahmet Katı for his support in conducting the bacterial attachment tests.

Funding Open access funding provided by the Scientific and Technological Research Council of Türkiye (TÜBİTAK). This research was supported by the Research Coordination Office of the University of Health Sciences Turkey as part of a Master's Thesis project (project no 2019/042).

Data Availability The datasets used and/or analyzed during the current study are available from the corresponding author on reasonable request.

Declarations

Conflict of interest The authors have no competing interests to declare that are relevant to the content of this article.

References

1. S. Fahimirad, H. Abtahi, P. Satei, E. Ghaznavi-Rad, M. Moslehi, A. Ganji, Carbohydr. Polym. **259**, 117640 (2021)
2. M. Zhang, X. Zhao, Int. J. Biol. Macromol. **162**, 1414 (2020)
3. L.I.F. Moura, A.M.A. Dias, E. Carvalho, H.C. De Sousa, Acta Biomater. **9**, 7093 (2013)
4. A.E. Stoica, C. Chircov, A.M. Grumezescu, Molecules **25**, 2699 (2020)
5. S. Cascone, G. Lamberti, Int. J. Pharm. **573**, 118803 (2020)
6. X. Wang, B. Ding, B. Li, Mater. Today **16**, 229 (2013)
7. E. Gámez, H. Elizondo-Castillo, J. Tascon, S. García-Salinas, N. Navascues, G. Mendoza, M. Arruebo, S. Irusta, Nanomaterials **10**, 616 (2020)
8. C. Huang, X. Xu, J. Fu, D.-G. Yu, Y. Liu, Polymers **14**, 3266 (2022)
9. H. R. M. Rashdan and M. E. El-Naggar, in *Antimicrob. Dress.* (Elsevier, 2023), pp. 21–42
10. M. Salehi, K. Shahporzadeh, A. Ehterami, H. Yeganehfard, H. Ziaei, M.M. Azizi, S. Farzamfar, A. Tahersoltani, A. Goodarzi, J. Ai, A. Ahmadi, Fibers Polym. **21**, 1713 (2020)
11. R. Sanchez Diaz, J. Park, L. L. Rodrigues, P. D. Dalton, E. M. De-Juan-Pardo, and T. R. Dargaville, Adv. Mater. Technol. **7**, 2100508 (2022)
12. T. Fan, R. Daniels, AAPS PharmSciTech **22**, 205 (2021)
13. J. Pan, N. Liu, H. Sun, F. Xu, PLoS ONE **9**, e112885 (2014)
14. S.I. Jeong, A.-Y. Lee, Y.M. Lee, H. Shin, J. Biomater. Sci. Polym. Ed. **19**, 339 (2008)
15. Y. Jung, S. H. Kim, H. J. You, S.-H. Kim, Y. Ha Kim, and B. G. Min, J. Biomater. Sci. Polym. Ed. **19**, 1073 (2008)
16. E.M. Tottoli, R. Dorati, I. Genta, E. Chiesa, S. Pisani, B. Conti, Pharmaceutics **12**, 735 (2020)
17. S. Barrientos, O. Stojadinovic, M.S. Golinko, H. Brem, M. Tomic-Canic, Wound Repair Regen. **16**, 585 (2008)
18. L. Shanmugam, A.V. Anuja, S.K. Rajinikanth, P. J. Samuel, in *Ther. Proteins Hum. Dis*. ed. by F.K. Zahid Balouch (Springer Nature Singapore, Singapore, 2022), pp.29–49
19. A. Golchin, M.R. Nourani, Polym. Adv. Technol. **31**, 2443 (2020)
20. L.A. Schneider, A. Korber, S. Grabbe, J. Dissemond, Arch. Dermatol. Res. **298**, 413 (2007)
21. P. Sim, X.L. Strudwick, Y. Song, A.J. Cowin, S. Garg, Int. J. Mol. Sci. **23**, 13655 (2022)
22. E.M. Jones, C.A. Cochrane, S.L. Percival, Adv. Wound Care **4**, 431 (2015)
23. B.S. Nagoba, N.M. Suryawanshi, B. Wadher, S. Selkar, Wounds **27**, 5 (2015)
24. M. Liu, X.-P. Duan, Y.-M. Li, D.-P. Yang, Y.-Z. Long, Mater. Sci. Eng. C **76**, 1413 (2017)
25. F.N. Parın, U. Parın, ChemistrySelect **7**, e202104148 (2022)
26. Z.Ł Babalska, M. Korbecka-Paczkowska, T.M. Karpiński, Pharmaceuticals **14**, 1253 (2021)
27. R. Kapukaya, O. Ciloglu, Int. Wound J. **17**, 1159 (2020)
28. Z. Sayin, U.S. Ucan, A. Sakmanoglu, Biol. Trace Elem. Res. **173**, 241 (2016)
29. M.A. Gavilanes-Martínez, A. Coral-Garzón, D.H. Cáceres, A.M. García, Mycoses **64**, 1045 (2021)
30. P. Fatma Nur, T. Pınar, P. Uğur, Y. Ayşenur, E. Murat, and Y. Kenan, Mater. Today Commun. **29**, 102921 (2021).
31. N. Roy, N. Saha, T. Kitano, P. Saha, Soft Mater. **8**, 130 (2010)
32. E. Kahraman, E. Göker, J. Trace Elem. Med. Biol. **73**, 127043 (2022)
33. I. Sogut, S.O. Paltun, M. Tuncdemir, M. Ersoz, C. Hurdag, Can. J. Physiol. Pharmacol. **96**, 404 (2018)

34. L.L. Lima, T.B. Taketa, M.M. Beppu, I.M.D.O. Sousa, M.A. Foglio, Â.M. Moraes, Mater. Sci. Eng. C **100**, 493 (2019)
35. G.-M. Lanno, C. Ramos, L. Preem, M. Putrinš, I. Laidmäe, T. Tenson, K. Kogermann, ACS Omega **5**, 30011 (2020)
36. S. Ramakrishna, K. Fujihara, W.-E. Teo, T. Yong, Z. Ma, R. Ramaseshan, Mater. Today **9**, 40 (2006)
37. M. Bognitzki, W. Czado, T. Frese, A. Schaper, M. Hellwig, M. Steinhart, A. Greiner, J.H. Wendorff, Adv. Mater. **13**, 70 (2001)
38. A.W. Laramée, C. Lanthier, C. Pellerin, A.C.S. Appl, Polym. Mater. **2**, 5025 (2020)
39. G. Salimbeigi, R.N. Oliveira, G.B. McGuinness, J. Appl. Polym. Sci. **139**, 52131 (2022)
40. A. Yar, A. Karabiber, A. Ozen, F. Ozel, S. Coskun, Renew. Energy **162**, 1428 (2020)
41. N. Selvakumar, A. Azhagurajan, T. S. Natarajan, and M. Mohideen Abdul Khadir, J. Appl. Polym. Sci. **126**, 614 (2012)
42. Y.J. Tan, W.Y. Yeong, X. Tan, J. An, K.S. Chian, K.F. Leong, J. Mech. Behav. Biomed. Mater. **57**, 246 (2016)
43. T. Rihayat, Suryani, C. N. Fitriyani, Nurhanifa, J. P. Siregar, J. Jaafar, T. Cionita, and Fitria, IOP Conf. Ser. Mater. Sci. Eng. **788**, 012045 (2020)
44. K. Inthanon, D. Daranarong, P. Techaikool, W. Punyodom, V. Khaniyao, A.M. Bernstein, W. Wongkham, Stem Cells Int. **2016**, 1 (2016)
45. H. Cho, D. Han, K. Matsumura, S. Tsutsumi, S. Hyon, Biomaterials **29**, 884 (2008)
46. Z. Khatri, R. Nakashima, G. Mayakrishnan, K.-H. Lee, Y.-H. Park, K. Wei, I.-S. Kim, J. Mater. Sci. **48**, 3659 (2013)
47. W. L. Tham, B. T. Poh, Z. A. Mohd Ishak, and W. S. Chow, J. Appl. Polym. Sci. **133**, app.42850 (2016)
48. S. S. Shazleen, L. Y. Foong Ng, N. A. Ibrahim, M. A. Hassan, and H. Ariffin, Polymers **13**, 3226 (2021)
49. Q. Wei, D. Sun, R. Yang, Y. Wang, J. Zhang, X. Li, Y. Wang, J. Mater. Eng. Perform. **31**, 1338 (2022)
50. M.F. Abdullah, A. Andriyana, F. Muhamad, B.C. Ang, J. Polym. Res. **30**, 257 (2023)
51. J.M. Kim, S. Song, Y.J. Hwang, J.Y. Jang, S. Lee, D.-I. Shin, S.W. Lee, S. Jeong, S.-H. Kim, G.-R. Yi, Y.S. Choi, G. Lee, Compos. Part B Eng. **225**, 109262 (2021)
52. A. Ulu, S. Balcioglu, E. Birhanli, A. Sarimeseli, R. Keskin, S. Koytepe, B. Ates, J. Appl. Polym. Sci. **135**, 46575 (2018)
53. J.L. Parsons, M.E. Milberg, J. Am. Ceram. Soc. **43**, 326 (1960)
54. A. Budak, M. Gönen, J. Supercrit. Fluids **92**, 183 (2014)
55. H.-M. Wang, Y.-T. Chou, Z.-H. Wen, Z.-R. Wang, C.-H. Chen, M.-L. Ho, PLoS ONE **8**, e56330 (2013)
56. C.R. Kruse, M. Singh, S. Targosinski, I. Sinha, J.A. Sørensen, E. Eriksson, K. Nuutila, Wound Repair Regen. **25**, 260 (2017)
57. T. Cui, J. Yu, C. Wang, S. Chen, Q. Li, K. Guo, R. Qing, G. Wang, J. Ren, Adv. Sci. **9**, 2201254 (2022)
58. J.R. Sharpe, K.L. Harris, K. Jubin, N.J. Bainbridge, N.R. Jordan, Br. J. Dermatol. **161**, 671 (2009)
59. S. Sivakumar, R. Murali, D. Arathanaikotti, A. Gopinath, C. Senthilkumar, S. Kesavan, B. Madhan, Int. J. Biol. Macromol. **177**, 463 (2021)
60. B. Kaczmarek, O. Mazur, O. Miłek, M. Michalska-Sionkowska, A.M. Osyczka, K. Kleszczyński, Prog. Biomater. **9**, 115 (2020)
61. T. Ren, J. Gan, L. Zhou, H. Chen, Polymers **12**, 1729 (2020)
62. E. Pinho, M. Henriques, G. Soares, Cellulose **21**, 4519 (2014)
63. S. Tyeb, N. Kumar, G. B. A. Kumar, and V. Verma, Soft Mater. **20**, 379 (2022)
64. D.M. Castilla, Z.-J. Liu, O.C. Velazquez, Adv. Wound Care **1**, 225 (2012)
65. F. Dadkhah Tehrani, I. Shabani, and A. Shabani, Carbohydr. Polym. **281**, 119020 (2022)
66. R.B. Trinca, C.B. Westin, J.A.F. Da Silva, Â.M. Moraes, Eur. Polym. J. **88**, 161 (2017)
67. S. S. Letha, A. S. Kumar, N. U., and M. J. Rosemary, J. Text. Inst. **113**, 378 (2022)
68. K. Nuutila, E. Eriksson, Adv. Wound Care **10**, 685 (2021)
69. D. M. Fernandes, W. S. Barbosa, W. S. P. Rangel, I. M. M. Valle, A. Paula Dos S. Matos, F. G. Melgaço, M. L. Dias, E. Ricci Júnior, L. C. P. Da Silva, L. C. L. De Abreu, and M. Sato De S.B. Monteiro, Mater. Today Commun. **26**, 102173 (2021)
70. P.I. Morgado, A. Aguiar-Ricardo, I.J. Correia, J. Membr. Sci. **490**, 139 (2015)
71. J.-P. Chen, Y. Chiang, J. Nanosci. Nanotechnol. **10**, 7560 (2010)
72. S. Jiji, S. Udhayakumar, K. Maharajan, C. Rose, C. Muralidharan, K. Kadirvelu, Carbohydr. Polym. **245**, 116573 (2020)
73. M. Naseri-Nosar, S. Farzamfar, H. Sahrapeyma, S. Ghorbani, F. Bastami, A. Vaez, M. Salehi, Mater. Sci. Eng. C **81**, 366 (2017)
74. H. Adeli, M.T. Khorasani, M. Parvazinia, Int. J. Biol. Macromol. **122**, 238 (2019)
75. B. Felice, M.A. Sánchez, M.C. Socci, L.D. Sappia, M.I. Gómez, M.K. Cruz, C.J. Felice, M. Martí, M.I. Pividori, G. Simonelli, A.P. Rodríguez, Mater. Sci. Eng. C **93**, 724 (2018)
76. K. Govindasamy, N.A. Dahlan, P. Janarthanan, K.L. Goh, S.-P. Chai, P. Pasbakhsh, Appl. Clay Sci. **190**, 105601 (2020)
77. X. Lang, Z. Tang, Z. Wei, X. Wang, S. Long, G. Zhang, J. Yang, Q. Lin, J. Innov. Opt. Health Sci. **15**, 2250007 (2022)
78. E. Yüksel, A. Karakeçili, T.T. Demirtaş, M. Gümüşderelioğlu, Int. J. Biol. Macromol. **86**, 162 (2016)
79. Y. Kuroyanagi, R. Suzuki, M. Kuroyanagi, Open J. Regen. Med. **12**, 49 (2023)
80. S. Kondo, Y. Kuroyanagi, J. Biomater. Sci. Polym. Ed. **23**, 629 (2012)
81. T. T. Yuan, P. M. Jenkins, A. M. DiGeorge Foushee, A. R. Jockheck-Clark, and J. M. Stahl, J. Nanomater. **2016**, 1 (2016)
82. Y. Ahmadi, M. T. Siddiqui, Q. Mohd. R. Haq, and S. Ahmad, Arab. J. Chem. **13**, 2689 (2020)
83. T.D. Kumar, M.S. Gokul, R.A. James, J. Microbiol. Biotechnol. Mol. Biol. **4**, 1 (2019)
84. E. D. Farfán-García, A. Kilic, J. García-Machorro, M. E. Cuevas-Galindo, B. A. Rubio-Velazquez, I. H. García-Coronel, E. Estevez-Fregoso, J. G. Trujillo-Ferrara, and M. A. Soriano-Ursúa, in *Viral Parasit. Bact. Fungal Infect.* (Elsevier, 2023), pp. 733–754